IEEE Access
Multidisciplinary | Rapid Review | Open Access Journal

Received January 5, 2022, accepted January 10, 2022, date of publication January 14, 2022, date of current version February 11, 2022.

Digital Object Identifier 10.1109/ACCESS.2022.3143812

Analysis of the Electromagnetic Interaction Between Periodically Corrugated Transmission Lines Through the Mutual Capacitance and Mutual Inductance

CHIA HO WU[1], GUOBING ZHOU[1], PEIXUN MA[1], YU WU[1], KEJUN LI[1], LINFANG SHEN[1], QIAN SHEN[1], HANG ZHANG[1], JINHUA YAN[1], (Member, IEEE), YUN YOU[1], JIANQI SHEN[2], XIAOLONG WANG[1,3], CHIN-CHIH CHANG[4], (Member, IEEE), AND FANG HE[5], (Senior Member, IEEE)

[1]Department of Applied Physics, College of Science, Zhejiang University of Technology, Hangzhou 310023, China
[2]College of Optical Science and Engineering, Zhejiang University, Hangzhou 310058, China
[3]Key Laboratory of Quantum Precision Measurement of Zhejiang Province, College of Science, Zhejiang University of Technology, Hangzhou 310023, China
[4]Department of Computer Science and Information Engineering, Chung Hua University, Hsinchu 30012, Taiwan
[5]Zhaolong Interconnect Technology Company Ltd., Deqing, Huzhou 313200, China

Corresponding authors: Jinhua Yan (jinhua@zjut.edu.cn) and Xiaolong Wang (xlwang@zjut.edu.cn)

This work was supported in part by the National Natural Science Foundation of China under Grant 62075197 and Grant 61875175, and in part by the Natural Science Foundation of Zhejiang Province under Grant LQ21F010013.

ABSTRACT In this study, we established, for the first time, an equivalent circuit model for coupled subwavelength periodic microstrip lines (CSPMLs) over a wide frequency range. The circuit composed of two identical and parallel subwavelength periodic microstrip lines has two fundamental modes, i.e., odd and even modes. Based on the two fundamental modes, the finite element method (FEM) is used to extract the circuit parameters, especially the frequency-dependent behavior of the mutual capacitance and mutual inductance for the CSPMLs. The *S*-parameters evaluated by full-wave simulation and the circuit model were highly consistent with a maximum deviation of only 0.249 dB for transmission coefficient below 15GHz. Because of reduced the mutual capacitance and mutual inductance, the crosstalk between two adjacent microstrip lines could be suppressed by optimizing the subwavelength periodic structure. The measured characteristic impedances for differential and common signals of CSPMLs also agree well with the numerical results. Therefore, we expect that the application of circuit models of CSPMLs would accelerate the use of metamaterial technology in the existing high-speed circuit systems.

INDEX TERMS Corrugated transmission lines, crosstalk, differential signal.

I. INTRODUCTION

As the chip working speed increases, the massive data to be processed in the integrated circuit (IC) has increased greatly. In the high frequency or high-speed circuit systems, some issues such as how to increase the working frequency of signals or the transmission rate of digital signals, and to fill more loops and devices in the unit area of the circuit board pose very difficult problems to circuit designers. Due to the existence of mutual capacitance and mutual inductance between two transmission lines, the crosstalk becomes an inevitable topic in the high-speed circuit design. Furthermore, as the rise time of digital signals shortens, the increase of coupling length between lines will intensify the crosstalk. In order to analyze the crosstalk between two adjacent microstrip lines, many researchers used electromagnetic numerical methods, such as finite difference time domain (FDTD) and circuit model method, to quantitatively analyze the electromagnetic interference (EMI) of two microstrip lines [1]–[3]. Seeking an efficient method to

The associate editor coordinating the review of this manuscript and approving it for publication was Barbara Masini.

isolate the EMI between two transmission lines has always been a popular research subject. Among the methods for reducing the crosstalk between transmission lines, the most obvious approach is to make the spacing between transmission lines at least triple line width (3W rule) [4]. The quantitative analysis of the EMI under the condition of keeping the spacing between two transmission lines at triple line width has a very high reference value. Reference [5] discussed the variation of four port *S*-parameters of two parallel microstrip lines with frequency when the spacing between parallel microstrip lines changed from a single line width (1W) to a quadruple line width (4W). The commercial software and experimental measurement verified that the far-end crosstalk (FEXT) and near-end crosstalk (NEXT) could be reduced efficiently by increasing the spacing between the two microstrip lines. Recently, as the signal transmission rate and transmission distance increased, the 3W rule signal isolation method loses its advantage. Introducing excessive spacing in many parallel microstrip lines brings extra difficulties to the miniaturization of circuit area. Furthermore, as the transmission frequency of many communication systems begins to enter the millimeter wave frequency band, the first problem to circuit system design is the crosstalk between loops. Therefore, the efficient EMI isolation between the transmission lines is really an urgent requirement for the analog or digital systems. Among the electromagnetic interferences of adjacent loops, the FEXT shows the most severe interference. How to create a new transmission structure to effectively eliminate FEXT is a very important issue. More recently, many useful plans for eliminating FEXT and NEXT are proposed [6], [7]. In order to reduce the mutual capacitance between two microstrip lines for eliminating crosstalk, Reference [6] used a Green function method to analyze the mutual capacitance of two microstrip lines in unequal width and eliminated the EMI by changing the dielectric constant of the filling medium between two microstrip lines. Reference [7] analyzed the crosstalk between two coupled microstrip lines by FDTD, and the numerical result showed that a slot between two microstrip lines could effectively reduce the electromagnetic coupling between microstrip lines. In two parallel microstrip lines, different field distributions of odd and even modes in free space result in different phase velocities of the two modes, which is a first cause of FEXT. The odd- and even-mode capacitances of the coupled microstrip lines can be adjusted effectively by connecting a series of decoupling capacitors between two microstrip lines [8]. In this way, the difference between the phase velocities of the two fundamental modes becomes small, and the FEXT can be reduced to the range of tolerance of a circuit system.

Recently, introducing an isolation structure between two microstrip lines is a mainstream technology for suppressing EMI. For example, Ref. [9] reported that the NEXT could be reduced effectively by using a nonuniform microstrip line with both ends connected to resistors in between two parallel microstrip lines. However, there must be a large spacing between the two transmission lines and this shielding wire. This method provides a better isolation for NEXT, but the spacing between two signal lines exceeds the triple line width [9]. In Refs. [10]–[16], a via-stitch guard to isolate two microstrip lines of transmitting signals was utilized. This method, which introduced a via-stitch guard trace in between two microstrip lines for isolating EMI, has been extensively used for commercial products. Reference [10] built a lumped circuit model between the via-stitch guard trace and the signal transmission microstrip line in order to predict the crosstalk of two microstrip lines. In order that the precision of the circuit model can be improved, the circuit parameters of the circuit system were extracted by a 2D quasi-static electromagnetic field equation. The theoretical analysis and the experimental measurement were in consistence with each other [10]. In Ref. [14], the isolation structure between two microstrip lines was changed as a grounded serpentine guard trace. In this scheme, the experimental results showed that the new isolation structure could effectively reduce the EMI. The grounded guard trace has been extensively identified with industrial products, but the excessive spacing between grounded metal tubes is likely to induce resonant coupling of electromagnetic signals between two microstrip lines [15]. Additionally, if such a grounded guard trace is used in a thick circuit board, there will be a strong interaction between the electromagnetic field and the grounded metal tubes. Besides the role in isolating two single-end microstrip lines, this grounded guard trace can also be used for isolating differential microstrip lines [17], e.g., it can effectively suppress a rapid increase of common signal in the frequency domain. The grounded guard trace can control the low frequency interference between the transmission lines, and the spacing between the transmission lines will exceed the triple line width (or at least broaden). This is a severe challenge to miniaturization of circuit area. This isolation method is not very effective in the case of higher frequencies [18]. Generally speaking, for two conventional coupled microstrip lines, the ratio of mutual capacitance to self-capacitance is smaller than the ratio of mutual inductance to self-inductance, which leads directly to a greater FEXT. Therefore, some researchers introduced periodic structures along the microstrip line edge, and such periodic structures of two microstrip lines were embedded as a sandwich [19]. This method eliminates the difference between mutual capacitance ratio and mutual inductance ratio for reducing FEXT by increasing the mutual capacitance of two microstrip lines [19]. This crosstalk isolation method frees the spacing between microstrip lines from the constraint of 3W rule. The spacing between two microstrip lines can be controlled effectively. However, an obvious defect in this isolation method is that the NEXT increases rapidly compared with 3W rule. The system of two periodic microstrip lines is a groove structure, where the two periodic microstrip lines are embedded in each other. However, such an embedded groove structure is unfavorable for transmitting differential signals. Additionally, the characteristic impedance of this type of microstrip structure with periodic texture is still difficult to

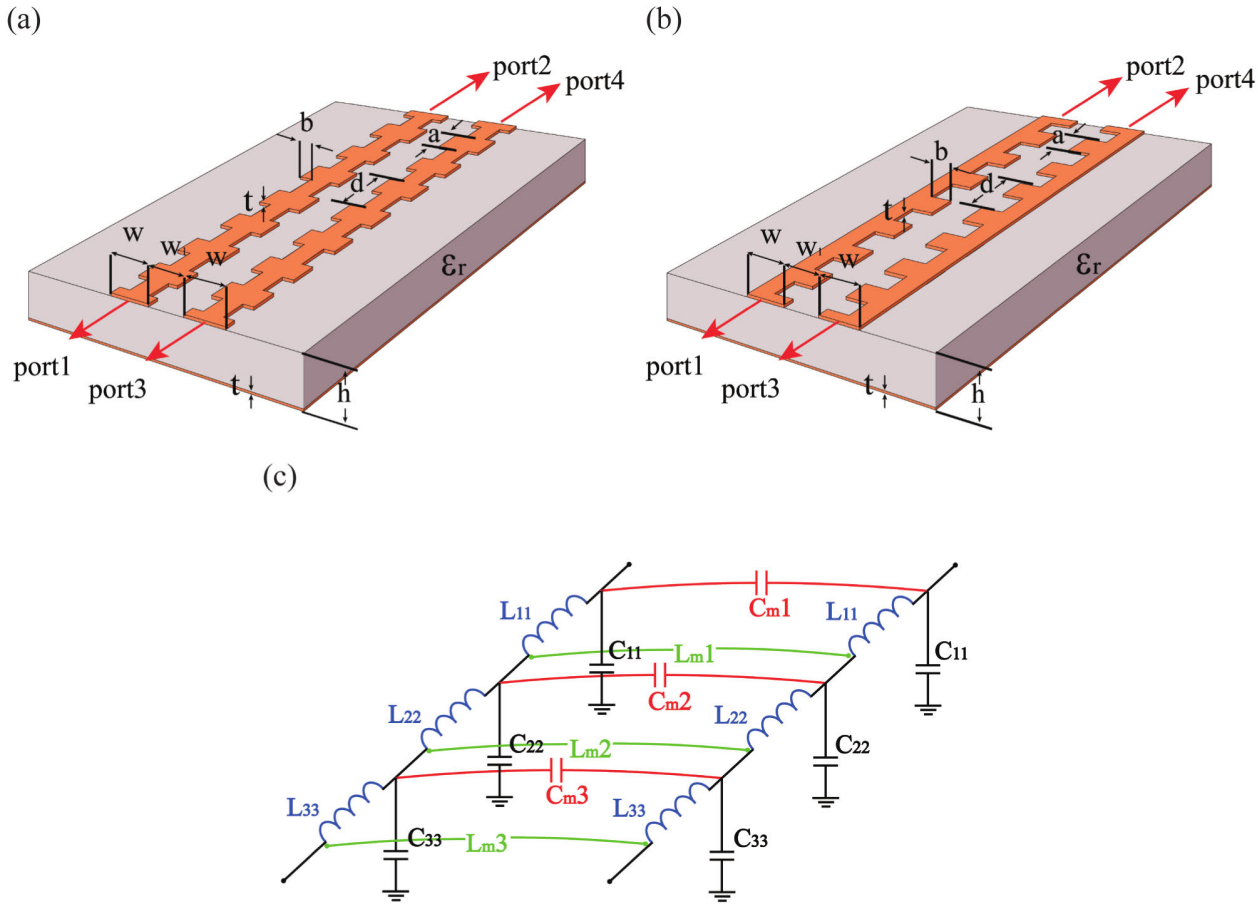

FIGURE 1. Schematic diagrams of the CSPMLs and their equivalent circuit model. (a) Coupled bilateral subwavelength periodic microstrip lines (CBSPMLs), (b)coupled unilateral subwavelength periodic microstrip lines (CUSPMLs), (c) equivalent circuit model of CSPMLs.

be determined theoretically. Thus, the periodic microstrip line cannot perform impedance matching with conventional microstrip line (CML), and the mutually embedded periodic microstrip line is not easy to be directly used, either, in many actual circuits. Therefore, the exploration of an accurate calculation method for the characteristic impedance of a microstrip line of this structure becomes a critical issue. In addition to the above method, in Refs. [20], a staircase structure was introduced into two microstrip lines for suppressing crosstalk. The introduction of subwavelength periodic corrugation into the microstrip line edge has been theoretically and experimentally proved available for effective isolation of EMI between microstrip lines [21]–[23], where the FEXT and NEXT can be eliminated simultaneously. The subwavelength periodic microstrip line (SPML) can effectively constrain the electromagnetic fields inside the microstrip line, and it is obviously different from the isolation methods of [19], [20]. The differential signal can be transmitted by using two equal-length parallel SPMLs together, and the generation of a common mode signal can be suppressed effectively [24]. In order to further reduce crosstalk, Ref. [25] introduced a guard trace of discontinuous construction in between two SPMLs to change the mutual capacitance and mutual inductance, so as to eliminate the FEXT of two periodic microstrip lines in the microwave and millimeter wave frequency bands. These SPMLs can effectively isolate the electromagnetic coupling between the microstrip lines, but there are still two key factors to be overcome in order to making use of the SPMLs in actual circuits. Then we are faced with two problems: First, whether it can be compatible with the existing technology and exceed the existing technology or not; second, whether or not a handy method can be provided for building an accurate circuit model, which can be combined with the circuit model of a transistor in the SPICE simulator to analyze the circuit system. Obviously, in terms of the SPML, the first factor is affirmative. However, the entire circuit system shall be simulated before practical uses, whether the circuit performance is satisfactory or not can be evaluated according to the simulation results. Therefore, a systematic method is required to provide the circuit parameters, characteristic impedance, mutual capacitance, and mutual inductance of the SPML. In terms of the conventional multiconductor transmission lines, the method of moment [26] and the finite element method based on quasi-static equation [27] are most frequently used for computing the relevant circuit parameters. However, these methods

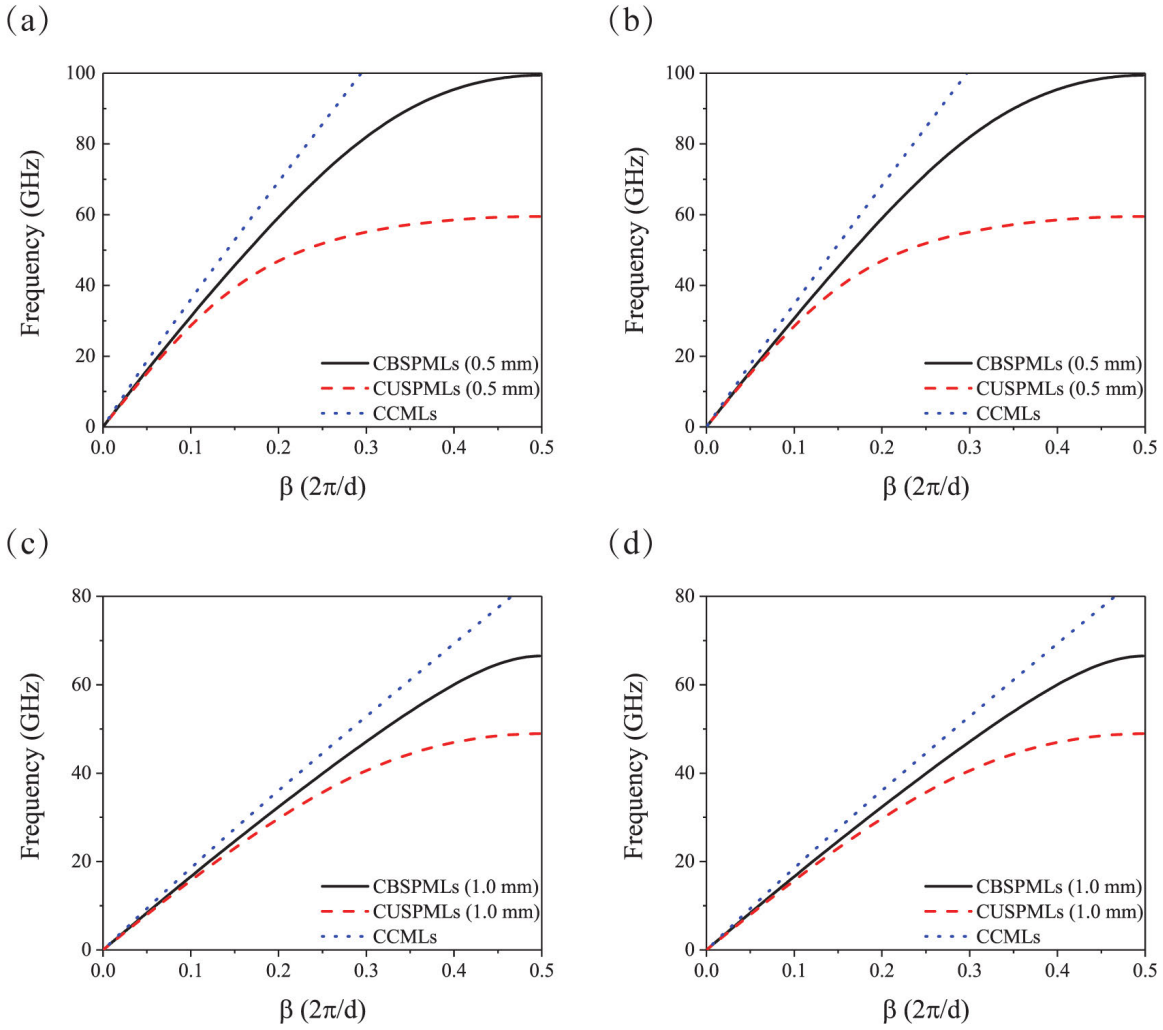

FIGURE 2. The dispersion curves of the CSPMLs for (a) odd modes with = 0.5 mm, (b) even modes with= 0.5 mm, (c) odd modes with= 1.0 mm, and (d) even modes with= 1.0 mm.

cannot provide circuit parameters that vary with frequency, nor can the commercial software.

The confinement effect of the SPML on EM field far exceeds that of the CML. Therefore, in actual circuits, based on SPMLs, many conventional planar transmission lines that undertake high-speed signal transmission can be replaced with microstrip lines as shown in Fig. 1. For a long time, the use of the circuit model to analyze the mechanism of CSPMLs to suppress crosstalk has been ignored by researchers. Therefore, our study explored the relevant circuit parameters behavior (especially the mutual capacitance and mutual inductance between two SPMLs) when the subwavelength periodic grooves are introduced at the edges of CMLs. The EMI suppression by the two SPMLs can be analyzed when we utilize the FEM to extract the frequency-dependent mutual capacitance and mutual inductance between the two SPMLs. The S-parameters were calculated using the circuit model and compared with the numerical result of the full-wave simulation. The numerical results of the characteristic impedances were also compared with the measured data of the time-domain reflectometer (TDR).

II. THEORETICAL ANALYSIS

The structures with two kinds of CSPMLs and their equivalent circuits are shown in Fig. 1. Two bilateral periodic corrugated microstrip lines and two unilateral periodic corrugated microstrip lines are presented in Fig. 1(a) and 1(b), respectively, with the geometrical parameters of line width w, groove depth b, lattice constant d, groove width $a = 0.5\ d$, metal thickness t, substrate thickness h, and dielectric constant ε_r. Considering the strong coupling, the space between the adjacent microstrip lines is set at $w_1 = w$. We used RO4003 as the substrate of the circuit with $h = 0.508$ mm, $\varepsilon_r = 3.37$, and $t = 0.0175$ mm. By setting $w =$ 1.2 mm, the characteristic impedance was close to 50 Ω. The groove depth was $b = 0.3\ w$ in Fig. 1(a) and $b = 0.6\ w$ in Fig. 1(b). Here, the lattice constant d was selected to be 0.5 mm, 1.0 mm, and 2.0 mm, which is the subwavelength dimension

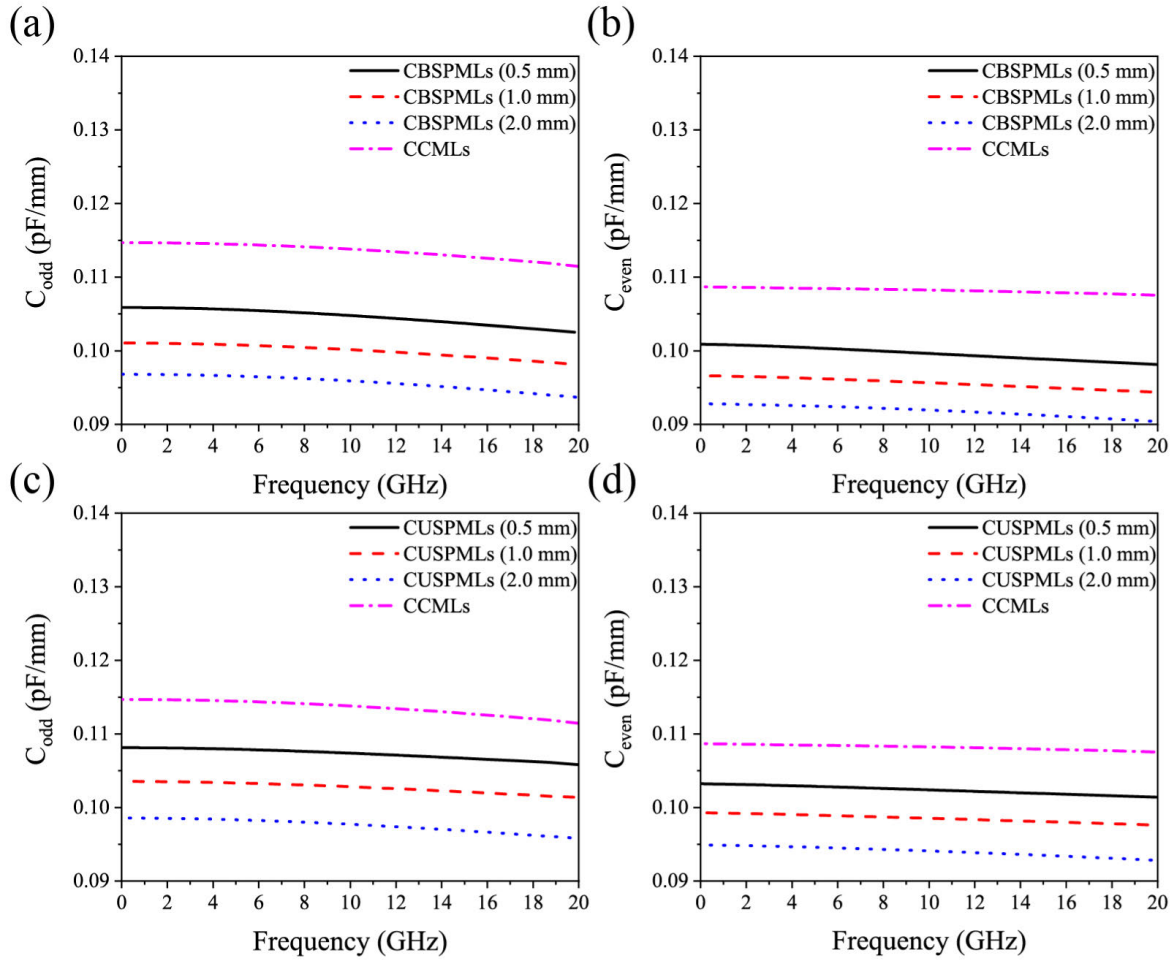

FIGURE 3. Per-unit-length capacitance of the CSPMLs for (a) odd modes in bilateral corrugations, (b) even modes in bilateral corrugations, (c) odd modes in unilateral corrugations, and (d) even modes in unilateral corrugations.

to suppress the mutual coupling. Particularly, it has been proved that such subwavelength periodic structures at the edge of the microstrip line help to suppress the EM coupling in the circuit board for even more thin trace [28]. The two coupled microstrip lines were identical and symmetric in geometric shape. Thus, the circuit parameters corresponding to even and odd modes could be calculated. The theoretical dispersion curves in the first Brillouin zone for $d = 0.5$ mm are shown in Figs. 2(a) and (b). For odd modes, the asymptotic frequency obtained by using the finite element method (FEM) was $f_{so} = 99.436$ GHz for the coupled bilateral subwavelength periodic microstrip lines (CBSPMLs), and $f_{so} = 59.493$ GHz for the coupled unilateral subwavelength periodic microstrip lines (CUSPMLs). For the even modes, the asymptotic frequency was $f_{se} = 99.441$ GHz for CBSPMLs, and $f_{se} = 59.496$ GHz for CUSPMLs. Figs. 2(c) and (d) show the dispersion bands for $d = 1.0$ mm. Here we have displayed the dispersion results of coupled conventional microstrip lines (CCMLs) as a comparison. We found that the asymptotic frequency decreased as the lattice constant d increased, leading to a weakened suppression effect. To obtain the equivalent circuit parameters, the distribution of electric charge Q in a unit cell for both odd and even modes were firstly calculated [29]. The voltage was obtained by the line integral of the electric field from the current return path to the signal trace as

$$V = -\int_0^h \vec{E} \cdot d\vec{l} \tag{1}$$

Consequently, the unit cell average capacitance can be expressed as

$$C = Q/V \tag{2}$$

The inductance is related to magnetic flux Φ as

$$L = \Phi/I \tag{3}$$

where I is the current in the microstrip line. Under the assumption $d \ll \lambda$, the approximation relation can be obtained as

$$v_p \approx \frac{1}{\sqrt{LC}} \tag{4}$$

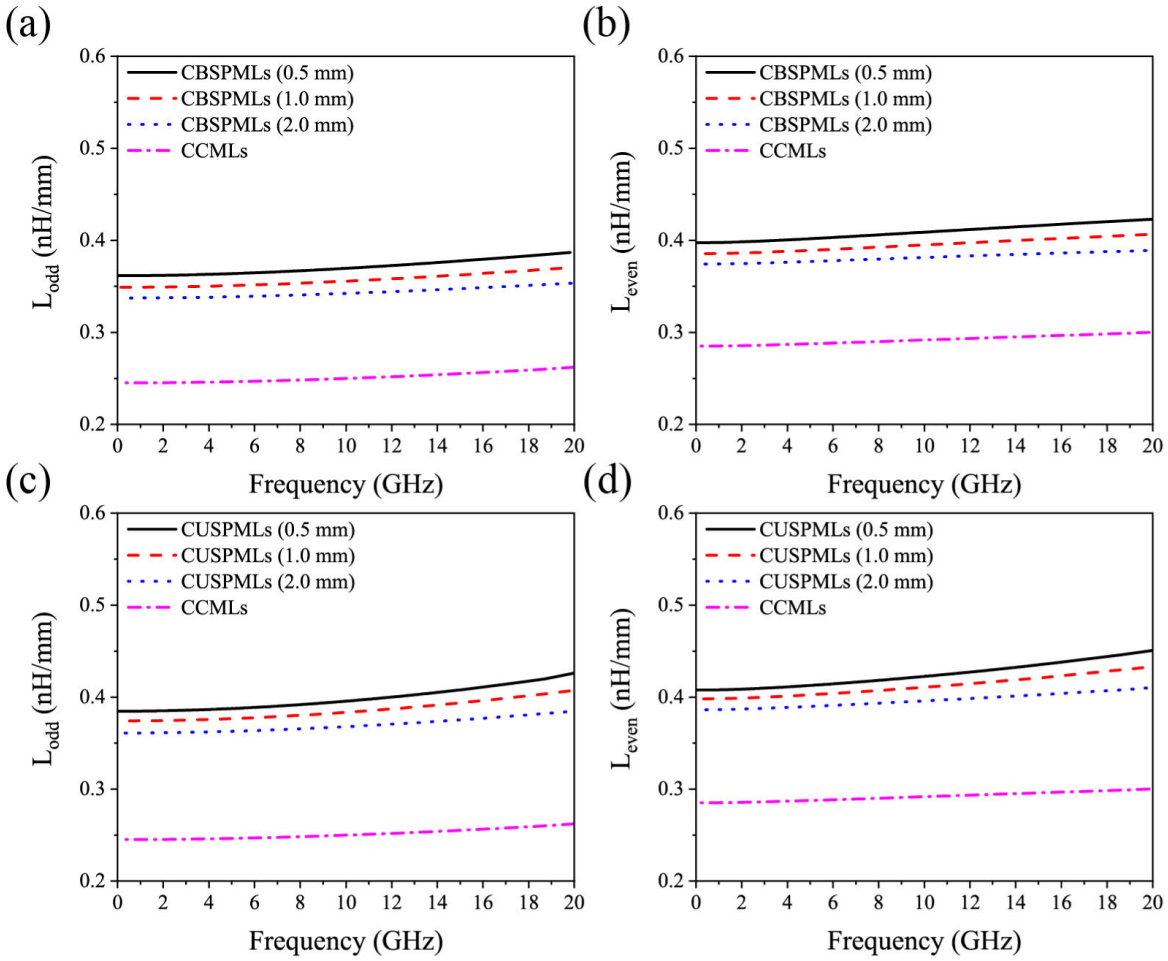

FIGURE 4. Per-unit-length inductance of CSPMLs for (a) odd modes in bilateral corrugations, (b) even modes in bilateral corrugations, (c) odd modes in unilateral corrugations, and (d) even modes in unilateral corrugations.

where v_p is the phase velocity in the microstrip line, and the equivalent circuit model was studied in [30]. COMSOL software is used to extract the related circuit parameters. Under the condition of low loss, the characteristic impedance of a single subwavelength periodic microstrip line can be obtained from the inductance and capacitance of a unit cell as follows

$$Z = \sqrt{\frac{L}{C}} \tag{5}$$

It should be noted that CSPMLs can be modeled by the equivalent circuit of infinite small conventional coupling transmission lines as shown in Fig. 1(c). The actual circuit model includes metallic resistance R and conductance G, which are omitted herein for the sake of concision. The calculation of circuit parameters is based on the approximation of quasi-TEM. In general, the equivalent circuit in the groove of the periodic microstrip line should correspond to a capacitance. However, the periodic structure of CSPMLs is the lattice constant d is much smaller than the wavelength, so there is no obvious electric potential difference between the two continuous protrusions in the periodic structure, that is, there exists no connected electric field lines between the two protrusions. Therefore, this capacitance can be omitted at low frequencies. On the other hand, the protruding part of the periodic structure should correspond to an inductance. If you are referred to the early papers on microstrip lines, you can find that a large amount of current in the microstrip line is transmitted along the edge of the conductor. The current flows in along one edge of the protrusion and flows out of the other edge. The net current flowing into the protrusion is zero. So there is no need to introduce additional inductance in the protrusion part of the periodic structure. It can be understood from the analysis of the COMSOL software that the magnetic field lines and the electric field lines of CSPMLs distribution is very similar to that of the coupled conventional microstrip lines, so the equivalent circuit model can be described by Fig. 1(c). We set a plane under the microstrip line for calculating the magnetic flux, and then obtain the inductance of the microstrip line through dividing the integral result (magnetic flux) by the current. In order to obtain the capacitance of the microstrip line, the electric flux passing through

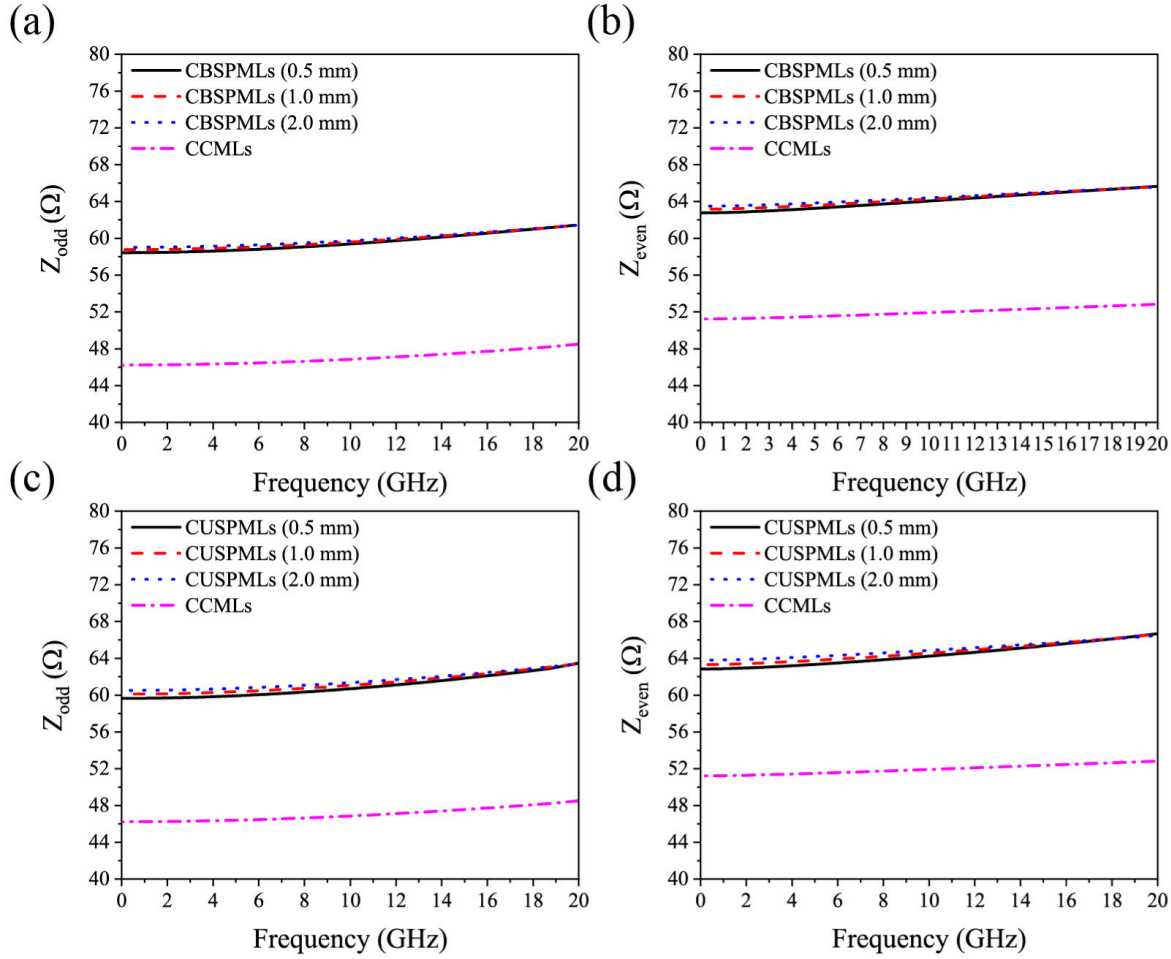

FIGURE 5. Characteristic impedance of the CSPMLs for (a) odd modes in bilateral corrugations, (b) even modes in bilateral corrugations, (c) odd modes in unilateral corrugations, and (d) even modes in unilateral corrugations.

a curved surface that contains the microstrip line will be calculated, and then the integral result (electric flux) divided by the voltage yields the capacitance. With the increase in frequency, such a simplified circuit model becomes invalid, and a more complex model is needed. At a low frequency, the construction of the circuit model needs to be based on the distribution of electric and magnetic fields in a unit cell of the subwavelength periodic structure. At frequencies between 0∼15G Hz, the magnetic field line is distributed around the transmission line, and there is no close-loop magnetic field line around the tab of the subwavelength periodic structure. Therefore, the introduction of an additional inductance along the direction of the tab is not required. Besides, as there are no connecting electric field lines between two tabs, the introduction of additional capacitance is not needed, and the circuit model of coupled conventional transmission lines suffices the requirement. For two parallel and identical microstrip lines, the eigenmodes are either odd mode or even mode. Under suitable boundary conditions, the above formula can be used to calculate the capacitance and inductance of the odd and even modes, respectively, of the coupled microstrip line. After the numerical results for inductance and capacitance have been obtained, the characteristic impedance of the corresponding modes can be calculated as follows:

$$Z_{odd} = \sqrt{\frac{L_{odd}}{C_{odd}}} \tag{6}$$

$$Z_{even} = \sqrt{\frac{L_{even}}{C_{even}}} \tag{7}$$

The per-unit-length capacitance for both coupled bilateral and unilateral corrugated microstrip lines is presented in Fig. 3. According to Fig. 3(a), the odd-mode capacitance for CCMLs is $C_{odd} = 0.11468$ pF/mm at $f = 0.05$ GHz, and it reduces slowly to $C_{odd} = 0.11279$ pF/mm at $f = 15$ GHz, with only 2% variation between 0∼15 GHz. For CBSPMLs with $d = 0.5$ mm, the odd-mode capacitance is a little smaller than the conventional one, which is $C_{odd} = 0.10588$ pF/mm at $f = 0.05$ GHz, and it drops gradually to $C_{odd} = 0.10371$ pF/mm at $f = 15$ GHz. Fig. 3(b) shows the per-unit-length capacitance for the even modes. For CCMLs, the capacitance is C_{even} =0.1087 pF/mm at

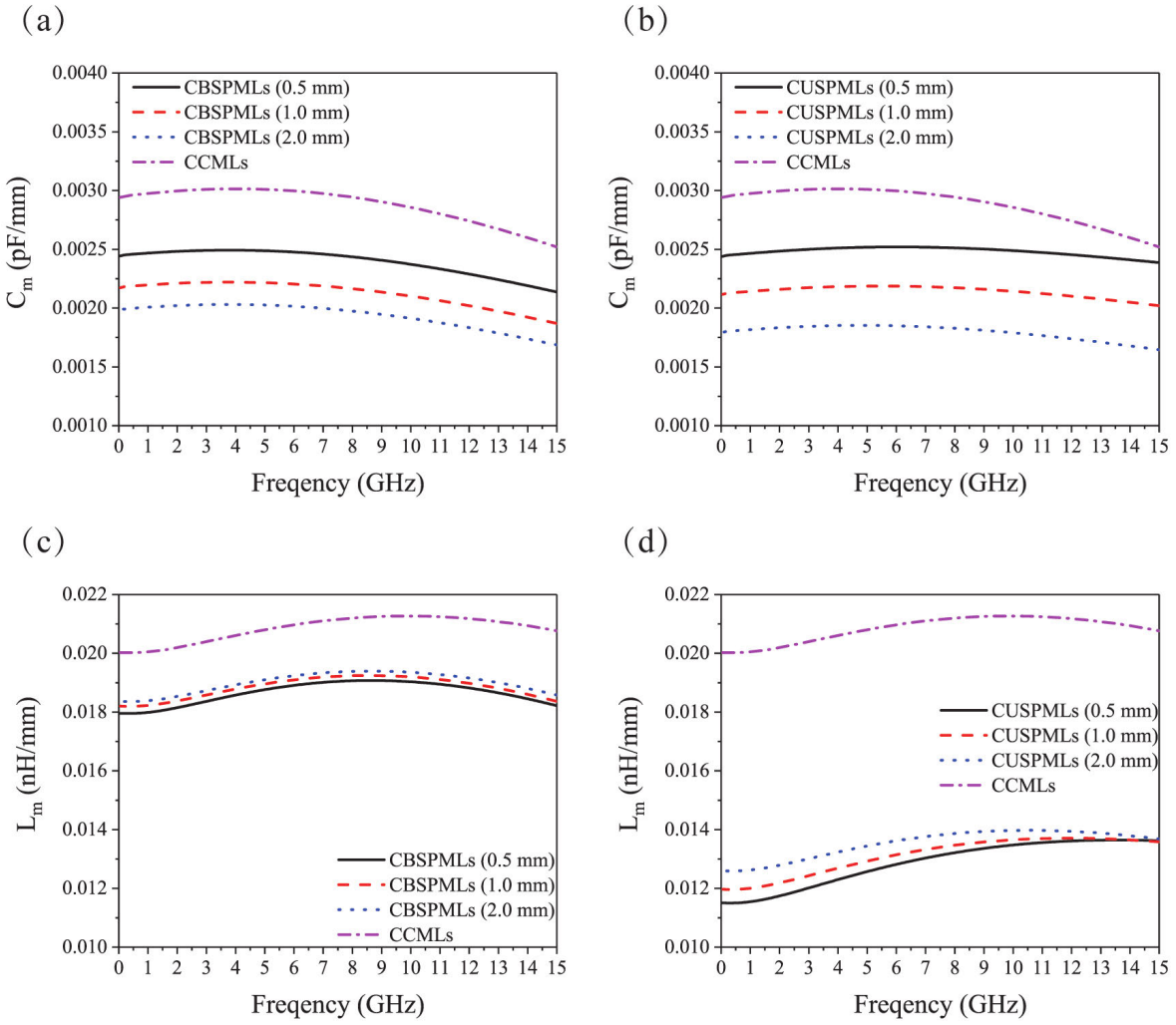

FIGURE 6. The frequency-dependent per-unit-length mutual capacitance and mutual inductance of the CSPMLs: (a) mutual capacitance in coupled bilateral corrugations, (b) mutual capacitance in coupled unilateral corrugations, (c) mutual inductance in coupled bilateral corrugations, and (d) mutual inductance in coupled unilateral corrugations.

$f = 0.05$ GHz, and drops slowly to $C_{even} = 0.10792$ pF/mm at $f = 15$ GHz. For the CBSPMLs with $d = 0.5$ mm, the even-mode capacitance is $C_{even} = 0.1009$ pF/mm at $f = 0.05$ GHz, dropping slowly to $C_{even} = 0.098872$ pF/mm at $f = 15$ GHz. In Fig. 3(c), the odd-mode capacitance for CUSPMLs is plotted. For $d = 0.5$ mm, the odd-mode capacitance is $C_{odd} = 0.10813$ pF/mm at $f = 0.05$ GHz, drops slowly to $C_{odd} = 0.10669$ pF/mm at $f = 15$ GHz. In Fig. 3(d) the even-mode capacitance for CUSPMLs is plotted. For $d = 0.5$ mm, the even-mode capacitance is $C_{even} = 0.10324$ pF/mm at $f = 0.05$ GHz, and decreases gradually to $C_{even} = 0.1019$ pF/mm at $f = 15$ GHz. It can be seen that the capacitance is almost constant in the band between 0.05∼15 GHz for the CSPMLs, and it decreases as the lattice constant d increases. Also, the even-mode capacitance is a little lower than that of the odd modes. In the case of the same frequency, the numerical difference between odd- and even-mode capacitances of CSPMLs is smaller than that of CCMLs, meaning that the mutual capacitance between the two SPMLs is smaller than that between two CMLs.

Fig. 4(a) shows the odd-mode per-unit-length inductance for CBSPMLs. For CCMLs, the inductance is $L_{odd} = 0.24516$ nH/mm at $f = 0.05$ GHz, and increases slowly to $L_{odd} = 0.25522$nH/mm at $f = 15$ GHz, with little variation in the frequency band under consideration. For CBSPMLs with $d = 0.5$ mm, the odd-mode inductance $L_{odd} = 0.36155$ nH/mm at $f = 0.05$ GHz, and increases slowly to $L_{odd} = 0.37756$ nH/mm at $f = 15$ GHz. Thus, the inductance value increases 4.2% within 0∼15 GHz. Obviously, because of the subwavelength scale grooves in the CSPMLs, the value of the inductance per-unit-length increases rapidly with the frequency. The capacitance per-unit-length of the CSPMLs gradually decreases with the frequency while the inductance increases, and the characteristics impedance can be expected to increase rapidly with the frequency. Fig. 4(b) shows the per-unit-length

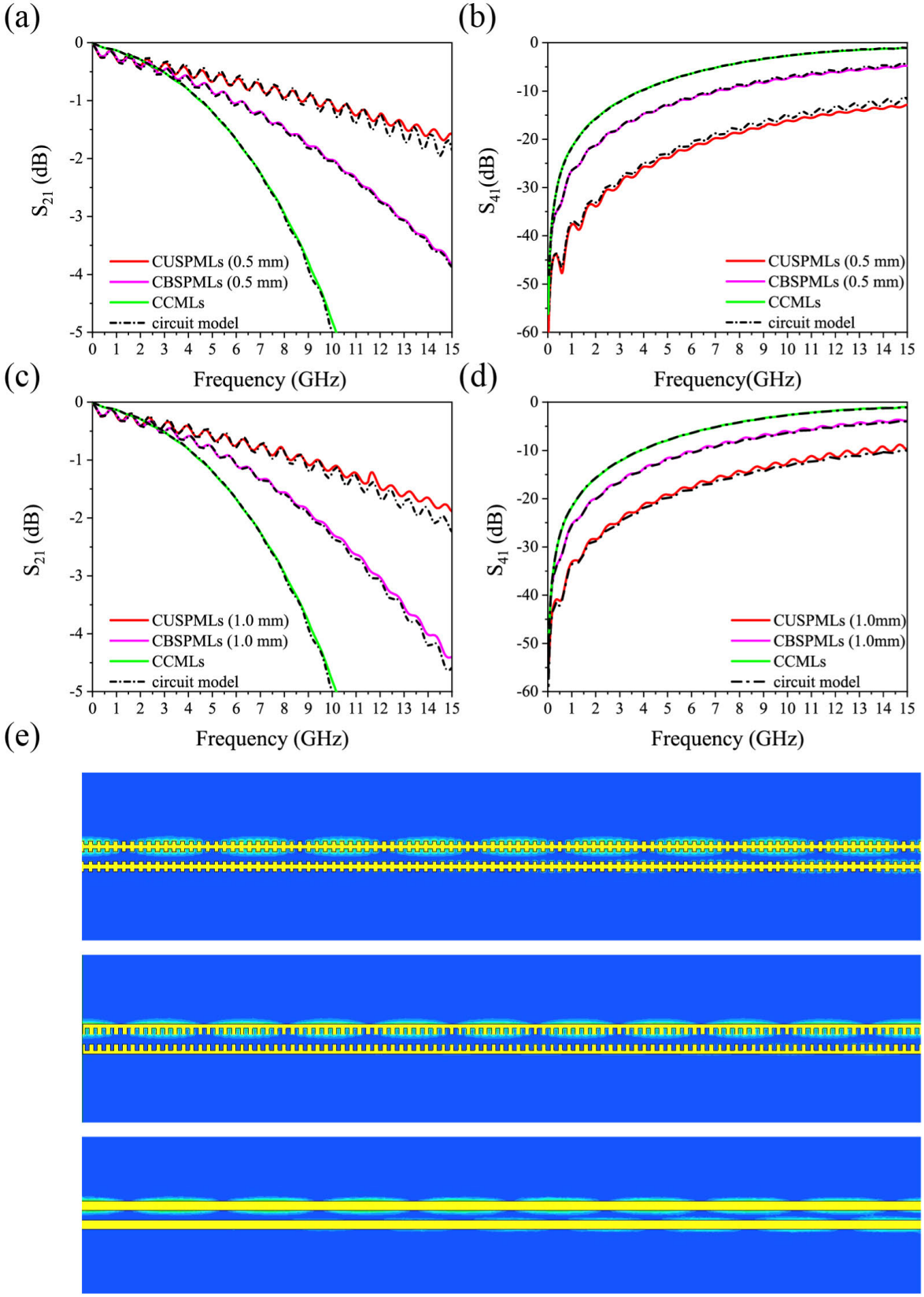

FIGURE 7. The S-parameters of the CSPMLs: (a) S_{21} for lattice constant $d = 0.5$ mm, (b) S_{41} for lattice constant $d = 0.5$ mm, (c) S_{21} for lattice constant $d = 1.0$ mm, (d) S_{41} for lattice constant $d = 1.0$ mm, and (e) field distribution of CSPMLs.

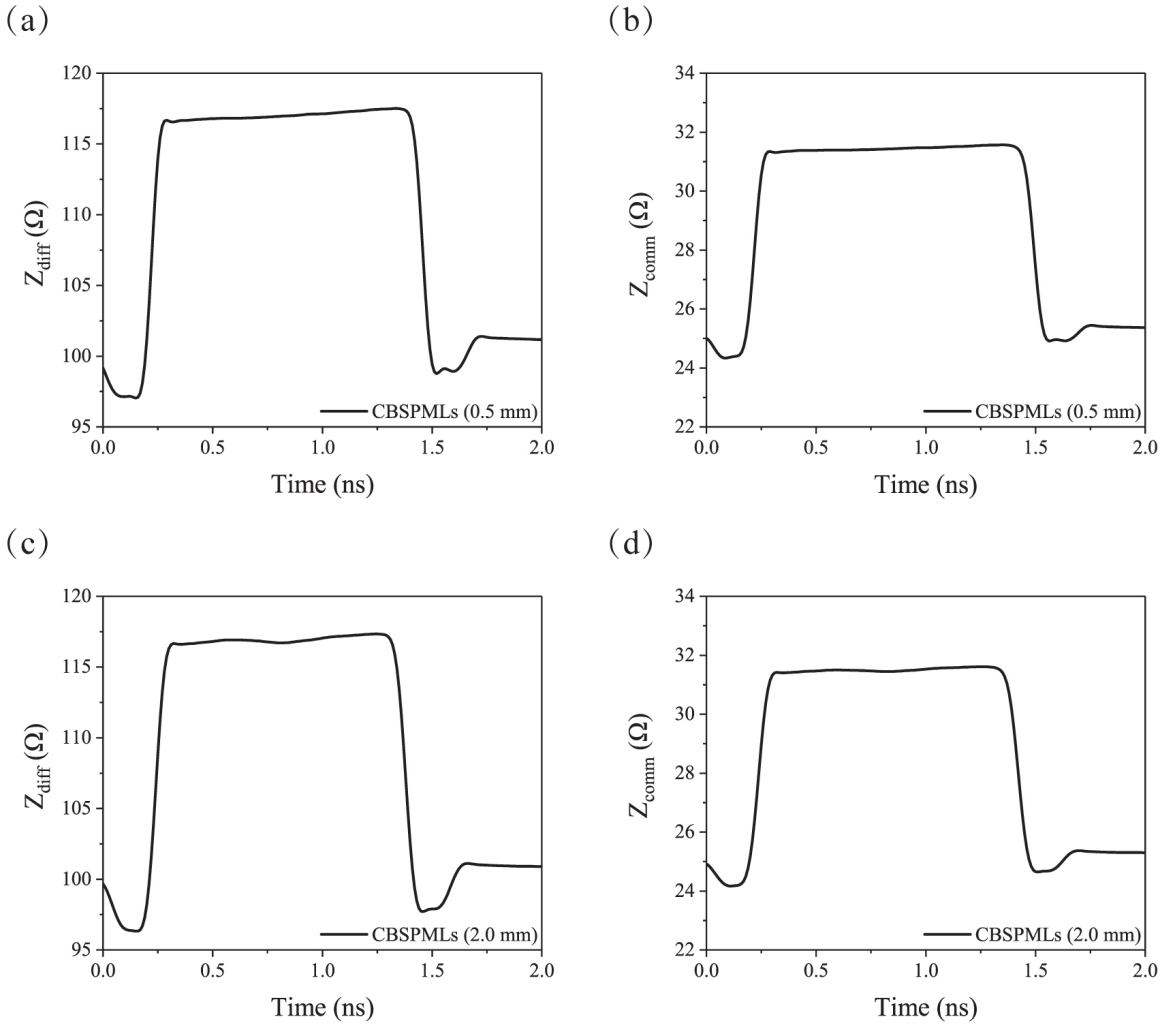

FIGURE 8. The Full-wave-simulation instantaneous impedances for CSPMLs for (a) differential signal instantaneous impedances of the CBSPMLs with $d = 0.5$ mm, (b) common signal instantaneous impedances of the CBSPMLs with $d = 0.5$ mm, (c) differential signal instantaneous impedances of the CBSPMLs with $d = 2.0$ mm, and (d) common signal instantaneous impedances of the CBSPMLs with $d = 2.0$ mm.

even-mode inductance of CBSPMLs. For CCMLs, the inductance is $L_{even} = 0.28519$ nH/mm at $f = 0.05$ GHz, increasing to $L_{even} = 0.29596$ nH/mm at $f = 15$ GHz. For CBSPMLs with $d = 0.5$ mm, the even-mode inductance $L_{even} = 0.39746$ nH/mm at $f = 0.05$ GHz, and it increases to $L_{even} = 0.41602$ nH/mm at $f = 15$ GHz. The odd-mode inductance for CUSPMLs is plotted in Fig. 4(c). For $d = 0.5$ mm, the odd-mode inductance is $L_{odd} = 0.3847$ nH/mm at $f = 0.05$ GHz, increasing to $L_{odd} = 0.40792$ nH/mm at $f = 15$ GHz. The even-mode inductance for CUSPMLs is presented in Fig. 4(d). From Fig. 4, it can be seen that the inductance of CSPMLs decreases with the increase of the lattice constant d, and this will lead to the deterioration of the of suppressing crosstalk. Also, the even-mode inductance is a little higher than that of the odd mode. The difference between odd-mode and even-mode inductances in coupled unilateral corrugations is smaller than that of coupled conventional and coupled bilateral corrugations, indicating that the smallest amount of the mutual inductance exists between the two unilateral periodic microstrip lines.

Fig. 5 presents the characteristic impedance for both coupled bilateral and coupled unilateral corrugated microstrip lines. According to Fig. 5(a), the odd-mode characteristic impedance for CCMLs is $Z_{odd} = 46.236\ \Omega$ at $f = 0.05$ GHz, and it increases to $Z_{odd} = 47.568\ \Omega$ at $f = 15$ GHz, with a little variation in the considered frequency band. For CBSPMLs with $d = 0.5$ mm, the odd-mode characteristic impedance $Z_{odd} = 58.437\ \Omega$ at $f = 0.05$ GHz, and it increases to $Z_{odd} = 60.338\ \Omega$ at $f = 15$ GHz, due to the subwavelength periodic structure in the microstrip line, where the characteristic impedance increases rapidly with the frequency. The characteristic impedance of CSPMLs has a little variation in the low frequency range while it increases fast in the high frequency range. The characteristic impedance for even modes

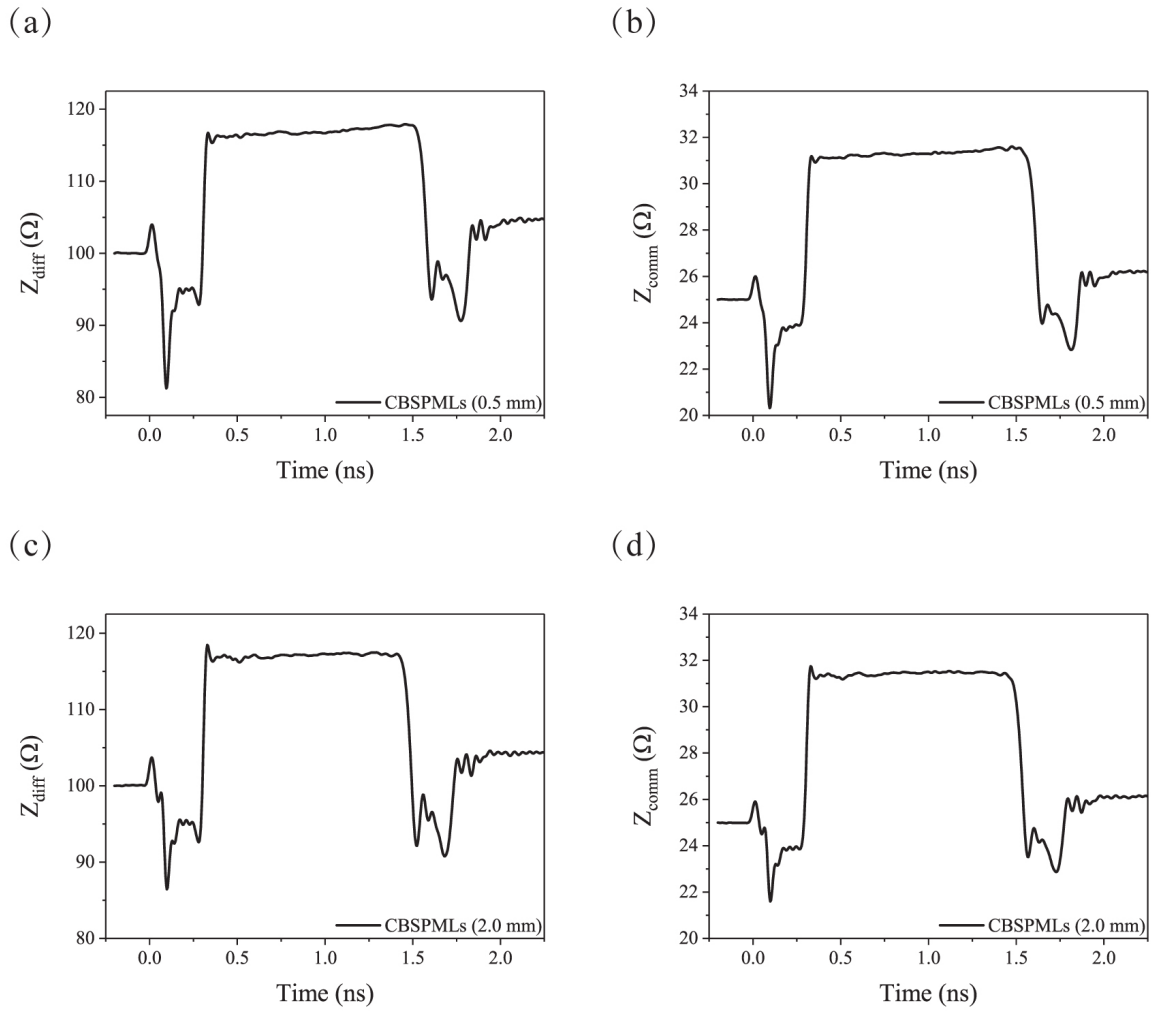

FIGURE 9. The measured instantaneous impedances for CSPMLs: (a) differential signal instantaneous impedances of the CBSPMLs with $d = 0.5$ mm, (b) common signal instantaneous impedances of the CBSPMLs with $d = 0.5$ mm, (c) differential signal instantaneous impedances of the CBSPMLs with $d = 2.0$ mm, and (d) common signal instantaneous impedances of the CBSPMLs with $d = 2.0$ mm.

in CBSPMLs is presented in Fig. 5(b). For CCMLs, the characteristic impedance is $Z_{even} = 51.22\ \Omega$ at $f = 0.05$ GHz, and it increases to $Z_{even} = 52.367\ \Omega$ at $f = 15$ GHz. For CBSPMLs with $d = 0.5$ mm, the even-mode characteristic impedance $Z_{even} = 62.761\ \Omega$ at $f = 0.05$ GHz, which increases to $Z_{even} = 64.867\ \Omega$ at $f = 15$ GHz. The odd-mode and even-mode characteristic impedance for CUSPMLs is plotted in Fig. 5(c) and (d).

In order to explain why the crosstalk between microstrip lines can be suppressed with the subwavelength periodic structure, by using the circuit model, we have calculated the mutual inductance and mutual capacitance between microstrip lines as described in a previous study [4]

$$C_m = \frac{C_{odd} - C_{even}}{2} \tag{8}$$

$$L_m = \frac{L_{even} - L_{odd}}{2} \tag{9}$$

Since the two parallel microstrip lines are identical, the mutual capacitance and mutual inductance of CSPMLs can be calculated in odd-mode and even-mode capacitance and inductance. The characteristic impedance of each microstrip line in the coupled circuit can be given by

$$Z_0 = \sqrt{\frac{L_{even} + L_{odd}}{C_{even} + C_{odd}}} \tag{10}$$

On the other hand, the capacitance and inductance matrices of the coupled periodic microstrip lines can be extracted directly from the COMSOL software, and the current I, voltage V, magnetic flux Φ and the accumulated charge Q of each microstrip line must be calculated according to equations (1) to (3). By substituting these variables (V and Q) into the following capacitance matrix, one can solve each matrix element (C_{ij}) in the equation set:

$$Q_1 = C_{11}V_1 + C_{12}(V_1 - V_2) \tag{11}$$

$$Q_2 = C_{22}V_2 + C_{21}(V_2 - V_1) \tag{12}$$

where C_{11} and C_{22} are self-partial capacitances and $C_{12} = C_{21}$ are mutual capacitance C_m. By inserting the relevant

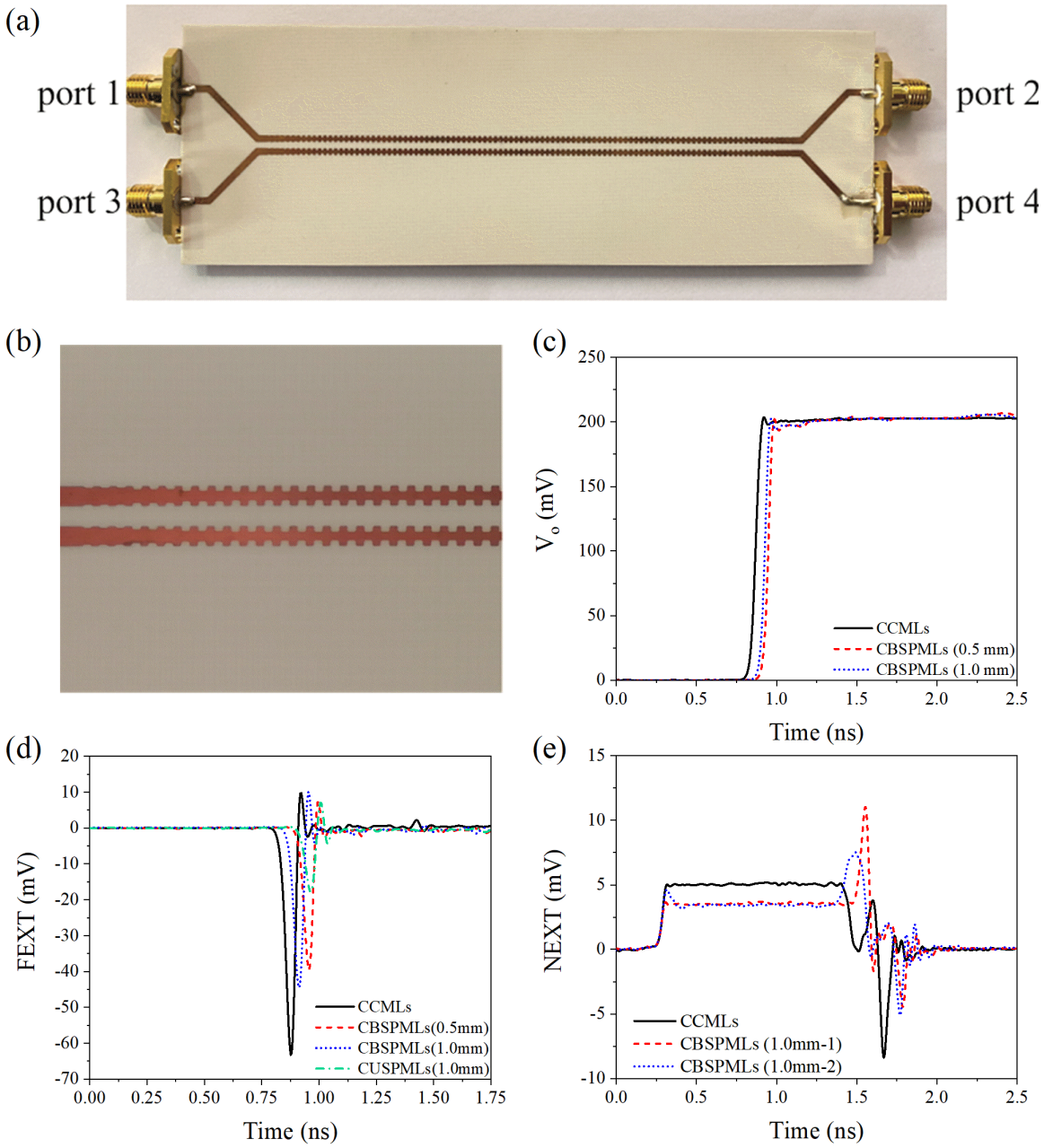

FIGURE 10. The measured time-domain signals of the CSPMLs for (a) the photo of CBSPMLs in the experiment, (b) the photo of CBSPMLs with input transition zone in the experiment, (c) the measurement of the output signal in port 2, (d) the measurement from FEXT in port 4, and (e) the measurement from NEXT in port 3.

variables (I and Φ) into the following inductance matrix, each element (L_{ij}) can also be solved:

$$\Phi_1 = L_{11}I_1 + L_{12}I_2 \tag{13}$$

$$\Phi_2 = L_{21}I_1 + L_{22}I_2 \tag{14}$$

where L_{11} and L_{22} are self-partial inductances and $L_{12} = L_{21}$ are mutual inductance L_m. Then the characteristic impedance of each microstrip line can be expressed as [32]

$$Z_0 = \sqrt{\frac{L_{11}}{C_{11} + C_{12}}} \tag{15}$$

The frequency-dependent per-unit-length mutual capacitance and mutual inductance for CSPMLs is shown in Fig. 6. The per-unit-length mutual capacitance for CBSPMLs is presented in Fig. 6(a), and the numerical result of CCMLs is also plotted as a comparison. The per-unit-length mutual capacitance of CBSPMLs is smaller than that of CCMLs, and the value decreases with the increase in lattice constant d, which can be explained by the smaller contribution of the fringe electric field to the per-unit-length capacitance and lower effective mutual capacitance due to a bigger surface area of the groove with a larger lattice constant d.

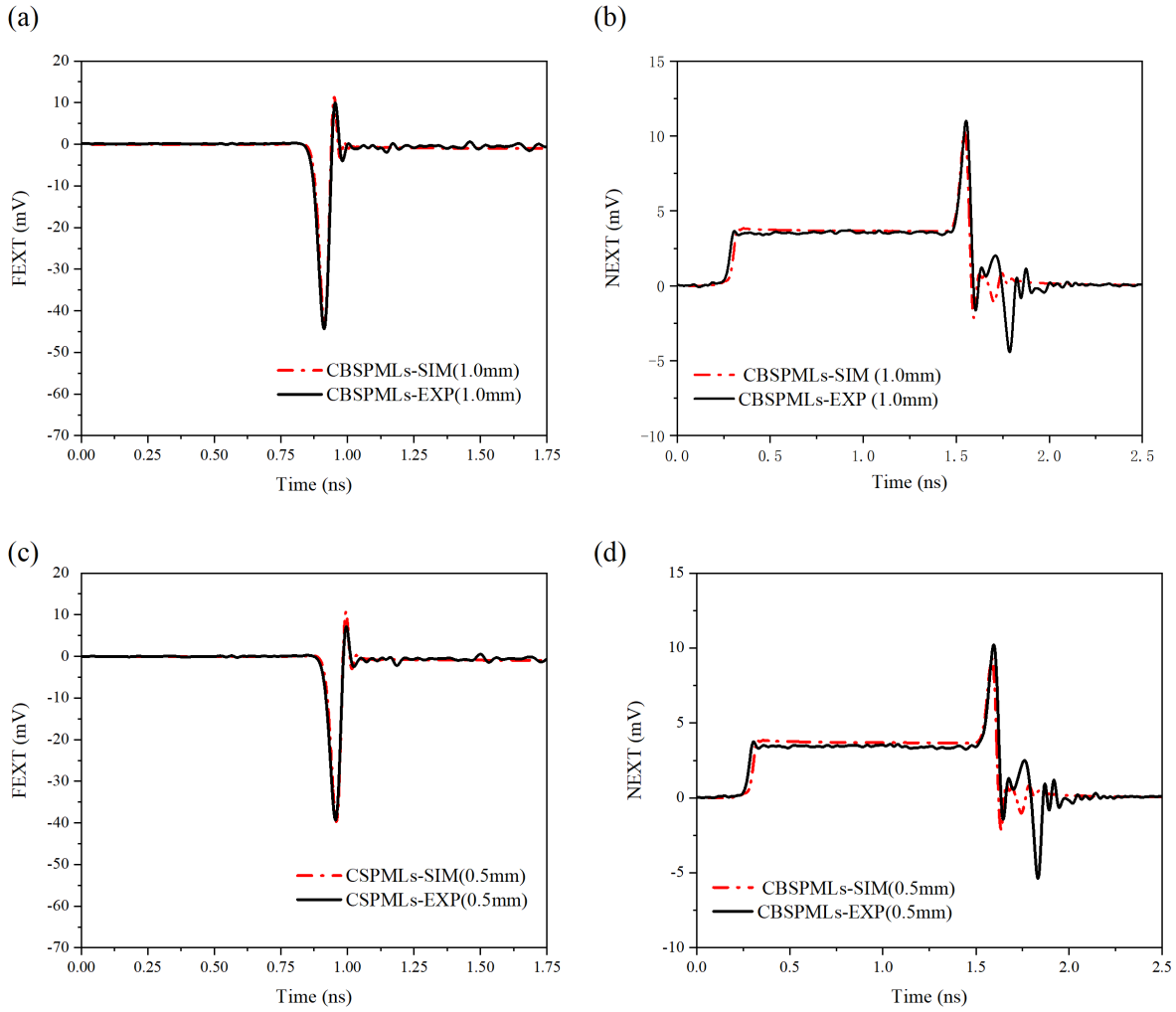

FIGURE 11. Comparison of the FEXT and the NEXT experimental measurement and simulation results of CSPMLs: (a) the FEXT measurement and simulation results of CBSPMLs with lattice constant $d = 1.0$ mm (b) the NEXT measurement and simulation results of CBSPMLs with lattice constant $d = 1.0$ mm, (c) the FEXT measurement and simulation results of CBSPMLs with lattice constant $d = 0.5$ mm, and (d) the NEXT measurement and simulation results of CBSPMLs with lattice constant $d = 0.5$ mm.

Fig. 6 (b) presents the per-unit-length mutual capacitance for CUSPMLs, where the numerical value is smaller than that of CBSPMLs at low frequencies. The per-unit-length mutual inductance for CBSPMLs is plotted in Fig. 6(c), of which the mutual inductance is much lower than that for CCMLs, since the self-inductance of the SPML is larger than that of the conventional one, which is beneficial for suppressing the crosstalk for digital signals. The per-unit-length mutual inductance for CUSPMLs is plotted in Fig. 6(d), which shows that the crosstalk can be suppressed more efficiently with the lowest mutual inductance. The lattice constant d as well as the groove depth b can be optimized to achieve the crosstalk suppression effectively. However, they also affect the characteristic impedance of the microstrip lines. Therefore, the use of SPMLs in actual circuits requires a careful selection of structural parameters to meet the needs of impedance matching. Next, we compared the S-parameters results from the circuit model with the full-wave simulation to verify our theoretical formalism.

The S-parameters for the CSPMLs at 10 cm length are given in Fig. 7, where red and purple lines represent the case of $d = 0.5$ mm and 1.0 mm, respectively. The input impedance was set at 50 Ω. This input impedance was adjusted to match the SPML's characteristic impedance for obtaining S_{21} with a smaller oscillation. The black-dash-dotted line represents the numerical results of the circuit model, and we observe that the CUSPMLs have much lower far-end crosstalk (S_{41}) compared with that of CBSPMLs. The full-wave simulation results agree well with that of the equivalent circuit model, with a deviation as small as 0.249 dB in S_{21} in our considered frequency range. It is clear that the suppression effect is more significant when the lattice constant d decreases. This leads S_{21} to drop slower with the increasing frequency. To improve the accuracy of S-parameters, we calculated the conductor resistance using the perturbation method [30], and the substrate dielectric conductance G was calculated according to the formula of dielectric-leakage resistance in Ref. [4]. Fig. 7 (e) shows

the field distribution of CSPMLs at 8 GHz. Obviously, the electromagnetic coupling of two microstrip lines can be suppressed effectively by introducing a subwavelength periodic structure into the edge of a microstrip line. According to the above data, as the SPML can effectively constrain the electromagnetic fields, it is suitable for long-distance transmission of signals on a circuit board.

Both odd and even modes exist in two parallel-coupled microstrip lines, where the differential and common signals excite the odd and even modes, respectively. As a result, odd- and even-mode characteristic impedance can be obtained with full-wave simulation. In the coupled microstrip lines, the detailed relation between the differential-signal and odd-mode characteristic impedances as well as the relation between the common-signal and even-mode characteristic impedances have been described in an earlier study [4]. They can be expressed as follows

$$Z_{diff} = 2Z_{odd} \tag{16}$$

$$Z_{comm} = Z_{even}/2 \tag{17}$$

As a result, the odd-mode and even-mode characteristic impedances can be obtained from differential and common signal characteristic impedances. Fig. 8 presents the numerical results of the instantaneous differential and common signal impedances through the full-wave simulation of CSPMLs, that is, the instantaneous impedances can be obtained by simulating the time domain reflectometer (TDR). An earlier study [31] indicated that the low frequency characteristic impedance of the microstrip lines could be measured using TDR, as the time of signal transmission in the microstrip line is greater than the rise time of a voltage pulse. Here we considered the case of CBSPMLs with $d = 0.5$ mm and $d = 2.0$ mm. A step function was used to excite the CSPMLs with a rise time of 30 ps. The full-wave simulation shows that the instantaneous impedances of differential and common signals were almost constant in the time rang 0.35∼1.42 ns, which means that the behavior of instantaneous impedance is similar between CSPMLs and CCMLs except for the values. The instantaneous impedance at any points on the transmission line is the same, which can be characterized as the characteristic impedance of the transmission line [4]. For CBSPMLs with $d = 0.5$ mm, the full-wave simulation of instantaneous impedance for the differential signal is 117.124 Ω at $t = 1$ ns, and it is 31.476 Ω for the common signal. The numerical results of Fig. 5 at low frequencies can be verified by the instantaneous impedance of the full-wave simulation. In such a low frequency range, the odd-mode characteristic impedance is 58.437 Ω, and the corresponding differential signal characteristic impedance is 116.874 Ω. The even-mode characteristic impedance at low frequency is 62.761 Ω, and the corresponding common signal impedance is 31.3805 Ω. The characteristic impedance deviation was only 0.213% for the differential signal, and 0.303% for the common signal between the circuit model and the full-wave simulation. For CBSPMLs with $d = 2.0$ mm, the instantaneous impedance for the differential signal is 117.0443 Ω at $t = 1$ ns, and it is 31.525 Ω for the common signal. At low frequencies, the odd-mode characteristic impedance is 59.022 Ω, and the corresponding differential signal impedance is 118.044 Ω. The even-mode characteristic impedance at low frequencies is 63.488 Ω, and the corresponding common signal impedance is 31.744 Ω. The characteristic impedance deviation is only 0.846% for the differential signal, and 0.705% for the common signal between the circuit model and the full-wave simulation. The odd-mode and even-mode characteristic impedances from the full-wave simulation and the equivalent circuit model were very consistent with each other.

III. EXPERIMENTAL RESULTS

To verify our theoretical investigation, we measured the differential and common signal instantaneous impedances of the CSPMLs by using the TDR method. Fig. 9 presents the measured instantaneous impedances for CSPMLs. According to Figs. 9(a) and (b), the measured experimental differential and common signal instantaneous impedances for CBSPMLs $d = 0.5$ mm are $Z_{diff} = 116.667$ Ω and $Z_{comm} = 31.295$ Ω at $t = 1$ ns, obtained from the numerical simulation, which is close to the values from the circuit model and full-wave simulation. For lattice constant $d = 2.0$ mm in Figs. 9(c) and (d), the experimental instantaneous impedances for differential and common signals are 117.28114 Ω and 31.5 Ω, respectively. As the circuit-model calculated characteristic impedance agrees well with that in the full-wave simulation, both methods can be utilized to calculate the characteristic impedance of the SPML, which makes the SPML characteristic impedance controllable and applicable in the planar circuits. Fig. 10 shows the crosstalk effect based on FEXT and NEXT measurement with input signal amplitude of 200 mV and the rise time of 30 ps. Fig. 10(a) presents the image of the circuit in our experiment, and Fig. 10(b) is the transition zone between CCMLs and CBSPMLs with a 1.0 cm length. In Fig.10(c), the step function signal at port 2 is given. As is observed, the digital signal transmission rate in the SPML is a little slower than that in a CML. The comparison of FEXT between CCMLs and CSPMLs is shown in Fig.10(d). For CCMLs, the peak value from FEXT is −63.282 mV, 31.6% of the input signal. For CBSPMLs with $d = 1.0$ mm, the peak value of FEXT is −43.44708 mV, 21.7% of the input signal. For CBSPMLs with $d = 0.5$ mm, the peak value of FEXT is −39.58132 mV, which is 19.79% of the input signal. For CBSPMLs, we observed that the FEXT value decreases only by 3.8657 mv when the lattice constant d changes from 1.0 mm to 0.5 mm, which is very small. For CUSPMLs with $d = 0.5$ mm, the peak value of FEXT is −15.6672 mV, which is only 7.83% of the input signal. As a result, the proposed subwavelength periodic structure can be used to suppress the crosstalk efficiently in the microstrip line circuits. Fig. 10(e) presents the measurement results of NEXT in CSPMLs. For CCMLs, the measured near-end crosstalk is 4.0 mV, which is 2.5% of the input signal. For CBSPMLs with

lattice constant $d = 1.0$ mm, the NEXT is 3.55 mV, which is 1.77% of input strength. For CCMLs, a big negative peak of -8.377 mV is observed at $t = 1.6675$ ns, which is the FEXT at port 3 from the port 2 reflection. However, this reflective FEXT is effectively suppressed in CBSPMLs. For CBSPMLs with $d = 1.0$ mm, its impedance mismatches with that of the CML, and an 11.036 mV voltage peak is observed at $t = 1.5541$ ns, such a voltage peak can be reduced to 7.52 mV with a 1.0 cm length transition zone at the input of CBSPMLs. As observed, the SPML can be used to suppress FEXT and NEXT effectively. To avoid a strong reflection induced by the impedance mismatch, it is beneficial to introduce a transition zone between the SPML and the CML. In order to compare the deviation between the experimental measurement and the simulation results, we used the CST commercial software to simulate FEXT and NEXT of CSPMLs and compared it with the experimental results, which are shown in Fig. 11. It can be clearly seen that the calculation results by the software are in good agreement with the experiment data.

IV. CONCLUSION

In this study, we have used the FEM to extract the circuit parameters (including the frequency-dependent mutual capacitance and inductance) of the CSPMLs from the unit cell of the periodic structure. The S-parameters for the circuit model agree well with the results from the full-wave simulation. For example, S_{21} from the two methods exhibited a maximum difference of 0.249 dB in the considered frequency band. The characteristic impedances measured from TDR agree with the numerical results of the full-wave simulation and the equivalent circuit model. The main advantage of introducing a subwavelength periodic structure at the edge of the CML is that it can dramatically reduce the mutual capacitance and mutual inductance with the adjacent loops. As a result, the FEXT and NEXT between two microstrip lines can be suppressed efficiently. The proposed circuit model can be applied directly to design of high-speed circuits with the CSPMLs. The grounded via holes of the grounded guard trace can make the wiring of the multilayer circuit board difficult, and even if the HDI technology is used, the spacing between the microstrip lines needs to be at least three times the width of the microstrip line. Compared with the grounded guard trace, our technology is obviously more flexible, because the spacing between two microstrip lines is not limited by three times the line width of the microstrip line, where any grounded via holes are not required. Therefore, the new technology will not cause the trouble of multi-layer circuit board wiring.

AUTHORS CONTRIBUTION

We are here to clarify the contribution of all the authors. The division of labor for all the authors is as follows: Chia Ho Wu proposed the idea and measured the circuit samples. Chia Ho Wu and Jinhua Yan prepared the article together. Jianqi Shen, Chin-Chih Chang, Qian Shen, Yun You, and Hang Zhang participated in the discussion of the research work for many times and pointed out the improprieties and errors in the article and helped to modify them. Guobing Zhou, Peixun Ma, Yu Wu, and Kejun Li participated in the extraction of the circuit parameters of the SPML circuit. Xiaolong Wang and Fang He provided measurement equipment and gave detailed views on the research plan. In particular, Fang He gave valuable suggestions on the application of SPML in actual circuits, playing the role of an engineer. Linfang Shen provided the perturbation calculation techniques, which were used to obtain the resistance of periodic microstrip lines.

ACKNOWLEDGMENT

The authors thank Prof. Song-Tsuen Peng (National Chiao-Tung University, Taiwan), Prof. Yu-Shan Li (Xidian University, Xi'an), Prof. Hai-Hui Zha and Prof. Hao Feng (Keysight Company Ltd., Shanghai), and Prof. Lei Shi (Ceyear Techologies Company Ltd., Qingdao) for their helpful discussions. They also thank Prof. Jianqing Shi and Prof. Qiang Lin for helping establishing the Microwave Measurement Laboratory.

REFERENCES

[1] F. Xiao, W. Liu, and Y. Kami, "Analysis of crosstalk between finite-length microstrip lines: FDTD approach and circuit-concept modeling," *IEEE Trans. Electromagn. Compat.*, vol. 43, no. 4, pp. 573–578, Nov. 2001.
[2] D. A. Hill, K. H. Cavcey, and R. T. Johnk, "Crosstalk between microstrip transmission lines," *IEEE Trans. Electromagn. Compat.*, vol. 36, no. 4, pp. 314–321, Nov. 1994.
[3] Y.-S. Sohn, J.-C. Lee, H.-J. Park, and S.-I. Cho, "Empirical equations on electrical parameters of coupled microstrip lines for crosstalk estimation in printed circuit board," *IEEE Trans. Adv. Packag.*, vol. 24, no. 4, pp. 521–527, Nov. 2001.
[4] E. Bogatin, *Signal Power Integrity: Simplified*, 2nd ed. Upper Saddle River, NJ, USA: Prentice-Hall, 2009, pp. 475–553.
[5] F. D. Mbairi, W. P. Siebert, and H. Hesselbom, "High-frequency transmission lines crosstalk reduction using spacing rules," *IEEE Trans. Compon. Packag. Technol.*, vol. 31, no. 3, pp. 601–610, Sep. 2008.
[6] S. He, A. Z. Elsherbeni, and C. E. Smith, "Decoupling between two conductor microstrip transmission line," *IEEE Trans. Microw. Theory Techn.*, vol. 41, no. 1, pp. 53–61, Jan. 1993.
[7] S. Dai, A. Z. Elsherbeni, and C. E. Smith, "Nonuniform FDTD formulation for analysis and reduction of crosstalk on coupled lines," *J. Electromagn. Waves Appl.*, vol. 10, no. 12, pp. 1663–1682, Jan. 1996.
[8] B.-R. Huang, K. C. Chen, and C. L. Wang, "Far-end crosstalk noise reduction using decoupling capacitor," *IEEE Trans. Electromagn. Compat.*, vol. 58, no. 3, pp. 836–848, Jun. 2016.
[9] L. Tani and N. E. Ouazzani, "Minimizing crosstalk on printed circuit board using non uniform guard traces," in *Proc. Int. Conf. Inf. Technol. Organizations Develop. (IT4OD)*, Mar./Apr. 2016, pp. 1–4.
[10] D. N. Ladd and G. I. Costache, "SPICE simulation used to characterize the cross-talk reduction effect of additional tracks grounded with vias on printed circuit boards," *IEEE Trans. Circuits Syst. II, Analog Digit. Signal Process.*, vol. 39, no. 6, pp. 342–347, Jun. 1992.
[11] I. Novak, B. Eged, and L. Hatvani, "Measurement and simulation of crosstalk reduction by discrete discontinuities along coupled PCB traces," *IEEE Trans. Instrum. Meas.*, vol. 43, no. 2, pp. 170–175, Apr. 1994.
[12] S. Li, Y. Liu, Z. Song, and H. Hu, "Analysis of crosstalk of coupled transmission lines by inserting additional traces grounded with vias on printed circuit boards," in *Proc. Asia–Pacific Conf. Environ. Electromagn. (CEEM)*, Nov. 2003, pp. 451–454.
[13] L. Zhi, W. Qiang, and S. Changsheng, "Application of guard traces with vias in the RF PCB layout," in *Proc. 3rd Int. Symp. Electromagn. Compat.*, Beijing, China, May 2002, pp. 771–774.
[14] W.-T. Huang, C.-H. Lu, and D.-B. Lin, "Suppression of crosstalk using serpentine guard trace vias," *Prog. Electromagn. Res.*, vol. 109, pp. 37–61, 2010.

[15] A. Suntives, A. Khajooeizadeh, and R. Abhari, "Using via fences for crosstalk reduction in PCB circuits," in *Proc. IEEE Int. Symp. Electromagn. Compat. (EMC)*, Portland, OR, USA, Aug. 2006, pp. 34–37.

[16] G.-H. Shiue, C.-Y. Chao, and R.-B. Wu, "Guard trace design for improvement on transient waveforms and eye diagrams of serpentine delay lines," *IEEE Trans. Adv. Packag.*, vol. 33, no. 4, pp. 1051–1060, Nov. 2010.

[17] F. D. Mbairi, W. P. Siebert, and H. Hesselbom, "On the problem of using guard traces for high frequency differential lines crosstalk reduction," *IEEE Trans. Compon. Packag. Technol.*, vol. 30, no. 1, pp. 67–74, Mar. 2007.

[18] D. J. Hou, J. J. Wi, C. J. Wu, J. Q. Shen, H. L. Chiueh, L. Y. Cheng, and H. E. Lin, "Experimental measure of transmission characteristics of low-frequency surface plasmon poaritons in frequency and time domains," *Opt. Exp.*, vol. 24, no. 7, pp. 7387–7397, 2016.

[19] S.-K. Lee, K. Lee, H.-J. Park, and J.-Y. Sim, "FEXT-eliminated tubal-ternated microstrip line for multi-gigabit/second parallel links," *Electron. Lett.*, vol. 44, no. 4, pp. 272–273, Feb. 2008.

[20] A. R. Mallahzadeh, A. Ghasemi, S. Akhlaghi, B. Rahmati, and R. Bayderkhani, "Crosstalk reduction using step shaped transmission line," *Prog. Electromagn. Res. C*, vol. 12, pp. 139–148, 2010.

[21] J.-J. Wu, "Subwavelength microwave guiding by periodically corrugated strip line," *Prog. Electromagn. Res.*, vol. 104, pp. 113–123, 2010.

[22] J. J. Wu, D. C. Tsai, T. J. Yang, H. E. Lin, H. L. Chiueh, L. Shen, I. J. Hsieh, J. Q. Shen, W. O. Yang, and Z. Gao, "Reduction of wide-band crosstalk for guiding microwave in corrugated metal strip lines with subwavelength periodic hairpin slits," *IET Microw., Antennas Propag.*, vol. 6, no. 2, pp. 231–237, Feb. 2012.

[23] X. Shen, T. J. Cui, D. F. Martin-Cano, and J. Garcia-Vidal, "Conformal surface plasmons propagating on ultrathin and flexible films," *Proc. Nat. Acad. Sci. USA*, vol. 110, no. 1, pp. 40–45, Jan. 2013.

[24] J. J. Wu, Da Jun Hou, K. Liu, L. Shen, C. A. Tsai, C. J. Wu, D. Tsai, and T.-J. Yang, "Differential microstrip lines with reduced crosstalk and common mode effect based on spoof surface plasmon polaritons," *Opt. Exp.*, vol. 22, no. 22, pp. 26777–26787, 2014.

[25] X. Dai, W. Feng, and W. Che, "Reduction of UWB far-end crosstalk in microwave and millimeter-wave band of parallel periodically loaded transmission lines with discontinuous structured guard lines," *IEEE Trans. Plasma Sci.*, vol. 48, no. 7, pp. 2372–2383, Jul. 2020.

[26] C. Wei, R. F. Harrington, J. R. Mautz, and T. K. Sarkar, "Multiconductor transmission lines in multilayered dielectric media," *IEEE Trans. Microw. Theory Techn.*, vol. MTT-32, no. 4, pp. 439–450, Apr. 1984.

[27] R. L. Khan and G. I. Costache, "Finite element method applied to modeling crosstalk problems on printed circuit boards," *IEEE Trans. Electromagn. Compat.*, vol. 31, no. 1, pp. 5–15, Feb. 1989.

[28] H. Takeda, K. Iokibe, and Y. Toyota, "Crosstalk suppression by introducing periodic structure into differential transmission lines," *IEICE Trans. Commun.*, vol. J101-B, no. 3, pp. 212–219, 2018.

[29] C. R. Paul, *Analysis of Multi-Conductor Transmission Lines*, 2nd ed. New York, NY, USA: Wiley, 2008.

[30] R. E. Collin, *Foundation for Microwave Engineering*, 2nd ed. New York, NY, USA: McGraw-Hill, 1992, pp. 550–551.

[31] K. S. D. Oh and X. C. C. Yuan, *High-Speed Signaling Jitter Modeling, Analysis, and Budgeting*. Upper Saddle River, NJ, USA: Prentice-Hall, 2012, pp. 121–136.

[32] S. H. Hall, G. W. Hall, and J. A. McCall, *High-Speed Digital System Design: A Handbook of Interconnect Theory and Design Practices*. New York, NY, USA: Wiley, 2000.

CHIA HO WU was born in Tainan, Taiwan. He received the M.S. degree in physics from the National Tsing Hua University, Hsinchu, Taiwan, in 1987, and the Ph.D. degree in electro-optics from Chiao Tung University, Hsinchu, in 1997. Since 2018, he has been a Professor with the Department of Applied Physics, College of Science, Zhejiang University of Technology, Hangzhou, China. His research interests include propagation and scattering of dielectric waveguides, numerical analysis of dielectric gratings, active leaky wave antennas, and subwavelength periodic metal structures.

GUOBING ZHOU was born in Huzhou, Zhejiang, China, in 1994. He received the B.S. degree from the Zhejiang University of Technology, Zhejiang, in 2017, where he is currently pursuing the master's degree. His research interests include microwave, millimeter-wave, and subwavelength periodic structures.

PEIXUN MA was born in Fuyang, Anhui, China, in 1997. He received the B.S. degree from the Anhui University of Technology, Anhui, in 2019. He is currently pursuing the master's degree with the Zhejiang University of Technology. His research interests include microwave, millimeter-wave, and subwavelength periodic structures.

YU WU received the B.S. degree in physics from Fuyang Normal University, Fuyang, China, in 2019. She is currently pursuing the M.S. degree with the College of Science, Zhejiang University of Technology, Hangzhou, China. Her current research interests include microwave theory, surface plasmon, and antennas.

KEJUN LI was born in Lishui, Zhejiang, China, in 1995. He received the B.S. degree from Huzhou University, Zhejiang, in 2019. He is currently pursuing the master's degree with the Zhejiang University of Technology. His research interests include microwave, millimeter-wave, and subwavelength periodic structures.

LINFANG SHEN was born in Zhejiang, China, in 1965. He received the B.S. degree in physics from Peking University, Beijing, China, in 1986, the M.S. degree in plasma physics from the Institute of Plasma Physics, Academy of Science of China, Hefei, China, in 1989, and the Ph.D. degree in electronic engineering from the University of Science and Technology of China, in 2000. He is currently a Professor with the Zhejiang University of Technology. His research interests include surface plasmonics, photonic crystals, and metamaterials.

QIAN SHEN was born in Sichuan, China, in September 1994. She received the B.S., M.S., and Ph.D. degrees from Nanchang University, Nanchang, China, in 2014, 2017, and 2020, respectively. Her research interests include surface magnetoplasmon, unidirectional wave transmission, and terahertz time domain spectroscopy.

HANG ZHANG was born in Zhejiang, China. He received the Ph.D. degree in physics from Zhejiang University, Hangzhou, China, in 2002. He is currently an Associate Professor with the Department of Applied Physics, College of Science, Zhejiang University of Technology, Hangzhou. His research interests include free form optical design, semiconductor illumination, and the propagation of subwavelength periodic metal structures.

JINHUA YAN (Member, IEEE) was born in Nantong, China. He received the B.S. degree in physics and the Ph.D. degree in optical engineering from Zhejiang University, Hangzhou, China, in 2002 and 2007, respectively. He is currently an Associate Professor with the Department of Applied Physics, College of Science, Zhejiang University of Technology, Hangzhou. His research interests include nano-photonic devices, numerical analysis of surface structure-based photonic devices, and optical sensing technique and application.

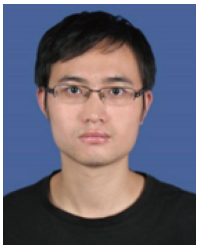

YUN YOU was born in Jiangxi, China, in 1990. He received the B.S., M.S., and Ph.D. degrees from Nanchang University, Nanchang, China, in 2012, 2015, and 2019, respectively. Since 2020, he has been working with the Department of Applied Physics, College of Science, Zhejiang University of Technology, Hangzhou, China. His research interests include surface magnetoplasmons, one-way waveguide, and 2D materials.

JIANQI SHEN was born in Xiaoshan, Hangzhou, Zhejiang, China, in November 1974. He received the Ph.D. degree from the Joint Research Centre of Photonics, Royal Institute of Technology, Sweden, and Zhejiang University, China. From 2006 to 2008, he was a Postdoctoral Researcher with Zhejiang University. He is currently an Associate Professor with the College of Optical Science and Engineering, Zhejiang University. His research interests include surface plasmonics, electromagnetic metamaterials, quantum optics, and related theoretical topics in classical and quantum field theories.

XIAOLONG WANG was born in Qingdao, China. He received the B.S. degree in physics from Zhejiang University, in 2006, and the Ph.D. degree in optics from Zhejiang University and the Ph.D. degree in physics from Paris Observatory, in 2011, following agreements between ministries of education of China and France. Since 2014, he has been working as an Assistant Professor with the College of Science, Zhejiang University of Technology. His research interests include atom interferometry, optical spectroscopy, and metamaterials.

CHIN-CHIH CHANG (Member, IEEE) received the M.S. degree in engineering science from the National Cheng Kung University, Tainan, Taiwan, in 1990, and the Ph.D. degree in computer science from Oklahoma State University, USA, in 2000. He is currently an Assistant Professor with the Department of Computer Sciences and Information Engineering, Chung Hua University, Hsinchu, Taiwan. His research interests include deep learning, recommendation systems, context-aware computing, sensor, and the Internet of Things (IoT) implementation.

FANG HE (Senior Member, IEEE) received the B.Eng. degree in communication engineering from Jilin University, Changchun, China, in 2002, and the M.Sc. degree in communication engineering and the Ph.D. degree in electrical and electronics engineering from The University of Manchester, Manchester, U.K., in 2005 and 2011, respectively.

Since 2009, he has been with HellermannTyton Data Ltd., Northampton, U.K., where he was the Product Development Engineer. Since 2019, he has been with Zhejiang Zhaolong Interconnect Technology Company Ltd., Deqing, China, where he is currently the Chief Specialist of Generic Cabling and the Laboratory Director.

Dr. He is a member of the Institution of Engineering and Technology (IET), U.K. He is also a Chartered Engineer from the Engineering Council, U.K.